COMPUTATIONAL METHODS IN APPLIED MATHEMATICS, Vol. 4 (2004), No. 4, pp. 410–430

A GENERALIZED RELAXATION METHOD FOR TRANSPORT AND DIFFUSION OF POLLUTANT MODELS IN SHALLOW WATER

A.I. DELIS

Department of Sciences, Division of Mathematics, Technical University of Crete
University Campus, Chania 73100, Crete, Greece
E-mail: adelis@science.tuc.gr

Th. KATSAOUNIS

Department of Applied Mathematics, University of Crete
Heraklion 71409, Crete, Greece
and
Institute of Applied and Computational Mathematics
FORTH, Heraklion 71110, Crete, Greece

Abstract — We present a numerical method based on finite difference relaxation approximations for computing the transport and diffusion of a passive pollutant by a water flow. The flow is modeled by the well-known shallow water equations and the pollutant propagation is described by a transport equation. The previously developed nonoscillatory relaxation scheme is generalized to cover problems with pollutant transport, in one and two dimensions and source terms, resulting in a class of methods of the first and the second order of accuracy in space and time. The methods are based on the classical relaxation models combined with a Runge–Kutta time splitting scheme, where neither Riemann solvers nor characteristic decompositions are needed. Numerical results are presented for several benchmark test problems. The schemes presented are verified by comparing the results with documented ones, proving that no special treatment is needed for the transport equation in order to obtain accurate results.

2000 Mathematics Subject Classification: 65M06; 76M20; 76B15.

Keywords: Shallow Water Equations, Relaxation Schemes, Finite Differences, TVD, Transport and Diffusion of Pollutant, Source Terms..

1. Introduction

Water quality modeling is a big and important area of research since it involves problems related to public safety. In this work we focused on the study of pollutant (or contaminant) movement and propagation in water flows. The shallow water model, that has been widely used to model the physical phenomena of water flows such as flood waves, dam-breaks, tidal flows in estuary and coastal water regions, and bore wave propagation in rivers, among others, is being used to provide the hydrodynamic background. Considerable effort has been devoted to the development of computational methods for that kind of fluid flow simulations,

and particular in the field of finite volumes for systems of conservation laws. There has been a growing trend in favor of Riemann or Godunov-type based methods constructed within the finite volume framework (refer, e.g., to [17] and [14]). Such methods are noted for their good conservation and shock capturing capabilities. More recently many methods have been proposed for the numerical approximation of solutions of hyperbolic conservations laws incorporating source terms, with the application to the shallow water equations, based on such methods (see, e.g., [2, 6, 8–10, 13, 16]) producing very accurate results.

The starting point of our investigation is the class of relaxation schemes, first introduced in [11], which are based on the relaxation approximation to the nonlinear conservation law, that has a linear convection term and needs neither a Riemann solver nor the characteristic decomposition and thus enjoys great simplicity. The idea is to use a local relaxation approximation to construct linear hyperbolic system with a stiff lower order term that approximates the original nonlinear system with a small dissipative correction.As pointed out in [15], *relaxation is a flux approximation* and *relaxation linearizes the Riemann problem.* This simplicity can be of great significance when one has to solve large-scale engineering problems. The amount of computational and theoretical results for the relaxation schemes found in the literature has grown since they were first introduced (see, e.g., [7, 12] and references therein).

Following the successful application of the relaxation schemes for solving numerically the shallow water equations in [7], in this work we are concerned with the advection and diffusion of a pollutant in the shallow water system, introduced with a transport equation for the concentration of pollutant. It is important to investigate the behavior of the pollutant on a discrete level when applying a finite volume scheme, such as the relaxation one, in terms of conservation, advection and diffusion. Moreover, one has to investigate the interaction with a nonflat topography. At the moment we are not aware of any other schemes applied to the specific problem, with the exception of [1], where a two times steps kinetic scheme was proposed, and [4, 5], where a hybrid finite volume-particle method is presented. Both of these approaches produced very accurate results. Hence, the objective of this work is to demonstrate, from the numerical point of view, some of the potential and some of the limitations of the relaxation schemes as we can observe when applied to the transport of pollutant model, since it has not been tested before.

In Section 2, we give a detailed presentation of the model we want to solve, in one and two dimensions. In Section 3, we present a relaxation model and a numerical scheme for one-dimensional equations. We investigate the performance of the relaxation scheme in one-dimensional problems in Section 4 and in Section 5 we present some results for the two-dimensional case.

2. Model equations

We start from the well-known one-dimensional shallow water equations, which represent mass and momentum conservation,

$$\begin{aligned} \frac{\partial h}{\partial t} + \frac{\partial (hu)}{\partial x} &= \Sigma(x,t), \\ \frac{\partial (hu)}{\partial t} + \frac{\partial}{\partial x}\left(hu^2 + \frac{gh^2}{2}\right) &= -gh\frac{\partial Z}{\partial x}. \end{aligned} \tag{1}$$

System (1) describes the flow at time $t \geqslant 0$ at point $x \in \mathbb{R}$, where $h(x,t) \geqslant 0$ is the total water height above the bottom, $u(x,t)$ is the average horizontal velocity, $\Sigma(x,t)$ denotes the sources of water (in m/s), $Z(x)$ is the bottom elevation (bed topography) function, and g the gravitational acceleration. In the following, we will denote as $q = hu$ the water unit discharge.

The propagation of a passive pollutant is modeled by the classical transport equation

$$\frac{\partial hC}{\partial t} + \frac{\partial (uhC)}{\partial x} = \Sigma C_\Sigma, \tag{2}$$

where $C(x,t)$ is the average pollutant concentration and C_Σ is a given concentration of the pollutant at the sources Σ. Pollutant transport models add extra species equations to the conventional shallow water equations. Here we consider the case of a single pollutant with concentration $C(x,t)$ transported with the water velocity, and following from (1), we may see this by deriving from (2) the following advection equation in the nonconservative form

$$\frac{\partial C}{\partial t} + u\frac{\partial C}{\partial x} = \Sigma(C_\Sigma - C)/h.$$

Equations (1) and (2) are coupled through the source terms and can be written in the form of a differential conservation law as a single vector equation

$$\frac{\partial \mathbf{U}}{\partial t} + \frac{\partial \mathbf{F}(\mathbf{U})}{\partial x} = \mathbf{S}(\mathbf{U}), \tag{3}$$

with

$$\mathbf{U} = \begin{pmatrix} h \\ q \\ Q_c \end{pmatrix}, \qquad \mathbf{F}(\mathbf{U}) = \begin{pmatrix} q \\ \frac{q^2}{h} + \frac{g}{2}h^2 \\ \frac{qQ_c}{h} \end{pmatrix}, \qquad \mathbf{S}(\mathbf{U}) = \begin{pmatrix} \Sigma \\ -gh\frac{\partial Z}{\partial x} \\ \Sigma C_\Sigma \end{pmatrix},$$

and we denote by $Q_c = hC$ the quantity of pollutant in the flow.

In the case where there are no sources of water ($\Sigma = 0$), we have a pure advection equation for the pollutant. For pure advection, equations (1) and (2) are decoupled automatically, since they are coupled by the source terms and can be solved independently. Nevertheless, the numerical scheme presented in the next section works in a unified way covering all cases.

For the hyperbolic system (3) there is an additional eigenvalue $\lambda_3 = u$ of the Jacobian matrix $\partial \mathbf{F}(\mathbf{u})/\partial \mathbf{u}$ (the other two, $\lambda_{1,2} = u \pm \sqrt{gh}$, are the same as those for the shallow water equations (1)). As pointed out in [17], use of the Riemann invariants for the characteristic field associated with this additional eigenvalue, shows that the pollutant concentration changes only on crossing a contact discontinuity defined by this eigenvalue. In this case, some numerical methods excessively smear the solution resulting in inaccurate predictions.

Assuming now that the flow is mainly two-dimensional, the model in its conservative form in 2D can be written as follows:

$$\frac{\partial \mathbf{U}}{\partial t} + \frac{\partial \mathbf{F}(\mathbf{U})}{\partial x} + \frac{\partial \mathbf{G}(\mathbf{U})}{\partial y} - \frac{\partial \widetilde{\mathbf{F}}(\mathbf{U})}{\partial x} - \frac{\partial \widetilde{\mathbf{G}}(\mathbf{U})}{\partial y} = \mathbf{S}(\mathbf{U}), \quad (x,y) \in \Omega, \tag{4}$$

with

$$\mathbf{U} = \begin{pmatrix} h \\ hu_1 \\ hu_2 \\ hC \end{pmatrix} = \begin{pmatrix} h \\ q_1 \\ q_2 \\ Q_c \end{pmatrix}, \quad \mathbf{S}(\mathbf{U}) = \begin{pmatrix} \Sigma(x,y,t) \\ -gh\frac{\partial Z}{\partial x}(x,y) \\ -gh\frac{\partial Z}{\partial y}(x,y) \\ \Sigma C_\Sigma \end{pmatrix},$$

$$\mathbf{F}(\mathbf{U}) = \begin{pmatrix} q_1 \\ \frac{q_1^2}{h} + \frac{1}{2}gh^2 \\ \frac{q_1 q_2}{h} \\ \frac{q_1 Q_c}{h} \end{pmatrix}, \qquad \mathbf{G}(\mathbf{U}) = \begin{pmatrix} q_2 \\ \frac{q_1 q_2}{h} \\ \frac{q_2^2}{h} + \frac{1}{2}gh^2 \\ \frac{q_2 Q_c}{h} \end{pmatrix},$$

$$\widetilde{\mathbf{F}}(\mathbf{U}) = \begin{pmatrix} 0 \\ 0 \\ 0 \\ hD_x\frac{\partial C}{\partial x} \end{pmatrix}, \qquad \widetilde{\mathbf{G}}(\mathbf{U}) = \begin{pmatrix} 0 \\ 0 \\ 0 \\ hD_y\frac{\partial C}{\partial y} \end{pmatrix},$$

where now $h(x,y,t) \geqslant 0$ is the height of the fluid at point (x,y) at time t, Ω denotes the projection of the domain occupied by the fluid onto the $x-y$ plane, and $Z(x,y)$ is again the bottom elevation, u_1, u_2 are the average velocity components of the water, with the invariant variables $q = (q_1, q_2)$ (with discharges) given by $q_1 = hu_1$, $q_2 = hu_2$, and finally D_x and D_y are diffusion coefficients.

It is well known that the solutions of systems (3) and (4) present steep fronts and shock discontinuities, which need to be resolved accurately in applications, and can cause severe numerical difficulties. Thus, computing numerical solutions is not trivial due to the nonlinearity, the presence of the convective term, and the coupling of the equations through the source terms.

3. Relaxation model and numerical scheme

The starting point for our investigation is the class of relaxation schemes first introduced in [11] for homogeneous conservation laws and their application in [7] to the shallow water equations with the geometrical source term present.

3.1. The relaxation model for 1D systems of conservation laws

Consider an extended (with a general source term present) nonlinear system of conservation laws in the following form:

$$\begin{aligned} \frac{\partial \mathbf{u}}{\partial t} + \frac{\partial \mathbf{f}(\mathbf{u})}{\partial x} &= \mathbf{s}(\mathbf{u}), \\ \mathbf{u}(x,0) &= \mathbf{u}_0(x), \end{aligned} \tag{5}$$

with the vector-value functions $\mathbf{u}$ and $\mathbf{f}(\mathbf{u})$ with values in $\mathbb{R}^n$. Introducing the artificial variable $\mathbf{v}$ (relaxation variable), the corresponding relaxation system is then given by

$$\begin{aligned} \frac{\partial \mathbf{u}}{\partial t} + \frac{\partial \mathbf{v}}{\partial x} &= \mathbf{s}(\mathbf{u}), \\ \frac{\partial \mathbf{v}}{\partial t} + \mathbf{C}^2\frac{\partial \mathbf{u}}{\partial x} &= -\frac{1}{\epsilon}\left(\mathbf{v} - \mathbf{f}(\mathbf{u})\right), \end{aligned} \tag{6}$$

with the initial data

$$\mathbf{u}(x,0) = \mathbf{u}_0(x),$$
$$\mathbf{v}(x,0) = \mathbf{v}_0(x) = \mathbf{f}(\mathbf{u}_0(x)),$$

where the small parameter ϵ is the *relaxation rate* ($0 < \epsilon \ll 1$) and

$$\mathbf{C}^2 = \mathrm{diag}\{c_1^2, c_2^2, \ldots, c_n^2\}$$

is a positive diagonal matrix to be chosen. For small ϵ, applying the Chapman-Enskog expansion to the relaxation system (6), we can derive the following approximation for $\mathbf{u}$:

$$\frac{\partial \mathbf{u}}{\partial t} + \frac{\partial \mathbf{f}(\mathbf{u})}{\partial x} = \mathbf{s}(\mathbf{u}) + \epsilon \frac{\partial}{\partial x}(\mathbf{f}'(\mathbf{u})\mathbf{s}(\mathbf{u})) + \epsilon \frac{\partial}{\partial x}\left((\mathbf{C}^2 - \mathbf{f}'(\mathbf{u})^2)\frac{\partial \mathbf{u}}{\partial x}\right), \tag{7}$$

where $\mathbf{f}'(\mathbf{u})$ is the Jacobian matrix of the flux $\mathbf{f}$. Equation (7) governs the first-order behavior of the relaxation system (6). Here we must require that the well-known *sub-characteristic condition*

$$\mathbf{C}^2 - \mathbf{f}'(\mathbf{u})^2 \geqslant 0, \quad \forall \mathbf{u}, \tag{8}$$

holds. This condition ensures the dissipative nature of (7). It is clear that for $\mathbf{u}$ varying in a bounded domain, equation (8) can always be satisfied by choosing sufficiently large values for $\mathbf{C}^2$. However, because of the stability constraints on a numerical scheme, it is desirable to obtain the smallest values for $\mathbf{C}^2$ meeting the criterion (8). The size of $\mathbf{C}^2$ has also a decisive influence regarding the numerical dissipation associated with the numerical schemes derived from (6). For both computational and theoretical purposes it is sometimes necessary to choose $\mathbf{C}^2$ to have distinct diagonal elements so as to avoid the degeneracy in the relaxation system. The construction of $\mathbf{C}^2$ must then be based on rough estimates of the characteristic speeds of the original problem. Hence, for the one-dimensional case we require that every eigenvalue λ_i of $\mathbf{f}'(\mathbf{u})$ should satisfy

$$|\lambda| \leqslant c_{\max}, \tag{9}$$

where $c_{\max} = \max_i c_i$. By doing so we insure that the characteristic speeds of the hyperbolic part of (6) are at least as large as the characteristic speeds of the original problem. Consequently, in the limit $\epsilon \to 0^+$ system (6) approaches the original system (5) by the *local equilibrium* $\mathbf{v} = \mathbf{f}(\mathbf{u})$.

The rigorous theory of kinetic approximation for solutions with shocks is well developed when the limit equation is scalar. In [15], it was shown that solutions of the relaxation model in the homogeneous system case converge strongly to the unique entropy solution of the original conservation laws. The relaxation model and its relaxation mechanisms, provide a subtle dissipative mechanism against the destabilizing effect of nonlinear response, as well as a damping mechanism on oscillations.

Using the system of n equations (5), we formulate the larger relaxation system (6) of $2n$ equations expressed as

$$\frac{\partial \mathbf{w}}{\partial t} + \frac{\partial \mathbf{H}(\mathbf{w})}{\partial x} = \mathbf{B}(\mathbf{w}), \tag{10}$$

where $\mathbf{w}, \mathbf{H}$, and $\mathbf{B} \in \mathbb{R}^{2n}$ and the new vectors are stated explicitly as

$$\mathbf{w} = \begin{pmatrix} u_1 \\ \vdots \\ u_n \\ v_1 \\ \vdots \\ v_n \end{pmatrix}, \quad \mathbf{H} = \begin{pmatrix} v_1 \\ \vdots \\ v_n \\ c_1^2 u_1 \\ \vdots \\ c_n^2 u_n \end{pmatrix}, \quad \text{and} \quad \mathbf{B} = \begin{pmatrix} s_1 \\ \vdots \\ s_n \\ -\frac{1}{\epsilon}(v_1 - f_1) \\ \vdots \\ -\frac{1}{\epsilon}(v_n - f_n) \end{pmatrix}.$$

We can see now that system (3) can easily be converted to the relaxation system (10) in a straightforward manner. We should note here that the characteristic variables are still much simpler than those of the nonlinear conservation law, since the relaxation system has linear characteristic variables, and that no information about the eigensystem of the Jacobian of the nonlinear flux is required, except for the upper bound of the largest eigenvalue in modulus, in order to adjust the parameters in $\mathbf{C}^2$ according to the subcharacteristic condition.

3.2. The relaxation scheme

To discretize the system of equations (10), we assume a space-uniform spaced grid with $\Delta x = x_{i+\frac{1}{2}} - x_{i-\frac{1}{2}}$ and a uniform time step $\Delta t = t^{n+1} - t^n, \quad n = 0, 1, 2, \ldots$ The approximate solution, denoted as the discrete value $\mathbf{w}_i^n$, is the approximate cell average of the variable $\mathbf{w}$ in the cell $(x_{i+\frac{1}{2}}, x_{i-\frac{1}{2}})$ at time $t = t^n$. The approximate point value of $\mathbf{w}$ at $x = x_{i+\frac{1}{2}}$ at time $t = t^n$ is denoted by $\mathbf{w}_{i+\frac{1}{2}}^n$.

A Runge–Kutta splitting scheme is defined as a five step iterative process for each vector $\mathbf{w}_i^n$ and is written in the following notation with the subscript i suppressed:

$$\mathbf{w}^{n,1} = \mathbf{w}^n + \Delta t \mathbf{B}(\mathbf{w}^{n,1}), \tag{11a}$$

$$\mathbf{w}^{(1)} = \mathbf{w}^{n,1} - \Delta t D_+ \mathbf{H}(\mathbf{w}^{n,1}), \tag{11b}$$

$$\mathbf{w}^{n,2} = \mathbf{w}^{(1)} - \Delta t \mathbf{B}(\mathbf{w}^{n,2}) - 2\Delta t \mathbf{B}(\mathbf{w}^{n,1}), \tag{11c}$$

$$\mathbf{w}^{(2)} = \mathbf{w}^{n,2} - \Delta t D_+ \mathbf{H}(\mathbf{w}^{n,2}), \tag{11d}$$

$$\mathbf{w}^{n+1} = \frac{1}{2}(\mathbf{w}^n + \mathbf{w}^{(2)}). \tag{11e}$$

This second-order implicit-explicit (IMEX) Runge–Kutta splitting scheme utilized here is different from the one presented for the shallow water equations in [7]. For the first n components of $\mathbf{w}$ in equations (11a) and (11c) one does not have to solve any implicit problems due to the special structure of the source term in equation (3) (following from (1)), while for the second n components one can again solve explicitly the above problem due to linearity of $\mathbf{v}$. For example, for the first n components of $\mathbf{w}^{n,1}$ in equation (11a) we have

$$u_i^{n,1} = u_i^n - \Delta t s_i(\mathbf{u}_i^{n,1}), \tag{12}$$

while for the second n components we have

$$v_i^{n,1} = v_i^n - \frac{\Delta t}{\epsilon}\left[f_i(\mathbf{u}_i^{n,1}) - v_i^{n,1}\right], \tag{13}$$

which we solve explicitly as

$$v_i^{n,1} = \frac{\left[v_i^n - \frac{\Delta t}{\epsilon} f_i(\mathbf{u}_i^{n,1})\right]}{\left(1 - \frac{\Delta t}{\epsilon}\right)}. \tag{14}$$

Hence, this splitting treats, alternatively, the stiff source terms $\frac{1}{\epsilon}(\mathbf{v}-\mathbf{f}(\mathbf{u}))$ implicitly in two steps because due to the structure of the source terms and the linearity of $\mathbf{v}$ one still solves them explicitly, and the convection terms with two explicit steps. Thus, we have an explicit implementation of an implicit source term, with stability constraints solely determined by the nonstiff convection terms, just as in a usual shock capturing scheme.

The spatial discretization is introduced in (11) by the operator

$$D_+\mathbf{H} = \frac{1}{\Delta x}(\mathbf{H}_{i+\frac{1}{2}} - \mathbf{H}_{i-\frac{1}{2}}).$$

To solve for $\mathbf{H}_{i\pm\frac{1}{2}}$ and construct a second-order accurate in space scheme, the MUSCL-TVD piecewise linear interpolation is applied to the kth component of $\mathbf{v}\pm\mathbf{Cu}$ to give respectively

$$\begin{aligned}(v+c_ku)_{i+\frac{1}{2}} &= (v+c_ku)_i + \frac{1}{2}\Delta x\sigma_i^+,\\ (v-c_ku)_{i+\frac{1}{2}} &= (v-c_ku)_{i+1} - \frac{1}{2}\Delta x\sigma_{i+1}^-,\end{aligned} \tag{15}$$

where u, v are the kth $(1 \leqslant k \leqslant n)$ components of $\mathbf{v}, \mathbf{u}$, respectively, the slopes in the ith cell are defined as

$$\sigma_i^{\pm} = \frac{1}{\Delta x}(v_{i+1} \pm c_ku_{i+1} - v_i \mp c_ku_i)\phi(\theta_i^{\pm}), \tag{16}$$

and

$$\theta_i^{\pm} = \frac{v_i \pm c_ku_i - v_{i-1} \mp c_ku_{i-1}}{v_{i+1} \pm c_ku_{i+1} - v_i \mp c_ku_i}, \tag{17}$$

where ϕ is a *limiter* function, satisfying

$$0 \leqslant \phi(\theta) \leqslant \text{minmod}(2, 2\theta). \tag{18}$$

There are several options on choosing a limiter function. Some of the most popular ones are the MinMod (MM) limiter

$$\phi(\theta) = \max(0, \min(1, \theta)),$$

the VanLeer (VL) limiter

$$\phi(\theta) = \frac{|\theta| + \theta}{1 + |\theta|},$$

the Superbee (SB) limiter

$$\phi(\theta) = \max(0, \min(2\theta, 1), \min(\theta, 2)),$$

and the Monotonized Central (MC) limiter

$$\phi(\theta) = \max(0, \min((1+\theta)/2, 2, 2\theta)).$$

Following from (15), we get

$$\begin{aligned}u_{i+\frac{1}{2}} &= \frac{1}{2}(u_i + u_{i+1}) - \frac{1}{2c_k}(v_{i+1} - v_i) + \frac{\Delta x}{4c_k}(\sigma_i^+ + \sigma_{i+1}^-),\\ v_{i+\frac{1}{2}} &= \frac{1}{2}(v_i + v_{i+1}) - \frac{c_k}{2}(u_{i+1} - u_i) + \frac{\Delta x}{4}(\sigma_i^+ - \sigma_{i+1}^-).\end{aligned} \tag{19}$$

slope $\sigma^{\pm} = 0$ or $\phi = 0$, the MUSCL scheme reduces to a *first-order upwind* scheme.

It is worth noting here that, in using the above schemes, neither a linear algebraic equation nor nonlinear source terms arise. In addition both the first- and the second-order relaxation schemes are stable under the *CFL* condition

$$\max\left((\max_i c_i)\frac{\Delta t}{\Delta x}\right) \leqslant 1. \tag{20}$$

In order to retain the TVD property (see [3, 11]) a more strict restriction has to be imposed on the usual *CFL* condition, and the one which was applied in the following section to calculate Δt

$$CFL = \max\left((\max_i c_i)\frac{\Delta t}{\Delta x}\right) \leqslant \frac{1}{2}.$$

4. 1D numerical tests and results

In this section, we illustrate the performance of the relaxation scheme by a number of numerical examples in 1D. In all tests the CFL number used was set to 0.5.

4.1. Initial and boundary conditions

For a given initial data $\mathbf{u}_0(x)$, for the above 1D relaxation system we choose the initial conditions in the form of

$$\begin{aligned}\mathbf{u}(x,0) &= \mathbf{u}_0(x),\\ \mathbf{v}(x,0) &= \mathbf{v}_0(x) \equiv \mathbf{F}(\mathbf{u}_0(x)).\end{aligned}$$

In the small relaxation limit ($\epsilon \to 0^+$), the relaxation system (10) satisfies the above. Hence, to avoid the introduction of an initial layer through the relaxation system the above initial value for $\mathbf{v}$ is chosen.

For the boundary conditions, given the physical boundary conditions, $\mathbf{u}_b$, that should be imposed for each problem, we set $\mathbf{v}_b = \mathbf{F}(\mathbf{u}_b)$ to avoid the introduction of artificial boundary layers. In general, any choice that leads at the limit to the associated boundary and initial equilibrium can be used.

The choices of c_i, $i = 1, 2, 3$, in all numerical tests are based on rough estimates of the eigenvalues $u \pm \sqrt{gh}, u$ of the Jacobian matrix $\partial\mathbf{F}(\mathbf{u})/\partial\mathbf{u}$ of the original equations, as to satisfy the sub-characteristic condition (9). Other choices can be made as long as numerical stability is maintained. It should be noted here that larger values for the c_i usually add more numerical viscosity, so for accuracy reasons it is desirable to have the c_i as small as possible. The relaxation parameter ϵ should be small with respect to the time step and space mesh length, that is, $\Delta t \gg \epsilon$ and $\Delta x \gg \epsilon$. Again here, ϵ plays the role of the viscosity coefficient so more numerical diffusion will be added for relatively larger values of ϵ.

The above ideas can be extended to the 2D case and are not presented here for brevity.

4.2. Advection of pollutant with constant discharge

As a first test problem, we consider the steady state problem in flat bottom ($Z = 0$) presented in [1]. Here the stationary solution of the shallow water equations has a constant discharge and the water height $h = 1m$. The channel length is $L = 500m$. The initial polluted area is $I = [20, 70]$ with $C_I(x, 0) = 1$, with no pollution source turned on. This polluted

area will be simply transported with the constant speed of the flow. As mentioned in [1], the numerical solution of this very simple problem clearly exhibits the influence of the Froude number, $Fr = \frac{u}{\sqrt{gh}}$, that characterizes whether the flow is subcritical ($Fr < 1$) or supercritical ($Fr > 1$). It also demonstrates the distinctions between the scheme diffusions in the numerical solutions obtained by the first order upwind relaxation scheme and the second order MUSCL scheme (using the SB limiter).

We computed solutions for different Fr values and the simulation time was in each case $t_{out} = \frac{100}{Fr}s$. The computational parameters used were $\Delta x = 5m, \epsilon = 1.D-6$. The values for the constants c_1, c_2 and c_3 have to be adjusted according to the flow parameters and we have set them for these problems, depending on the Fr value, equal to the values of $u + \sqrt{gh}, u - \sqrt{gh}$ and u respectively. The results are shown in Figs. 1 and 2. First the superiority of the second-order relaxation scheme can be clearly seen in all cases. The solution is only slightly diffused for the second-order scheme in all cases, and as the Fr number decreases (strongly sub-critical flow), the results are improving.

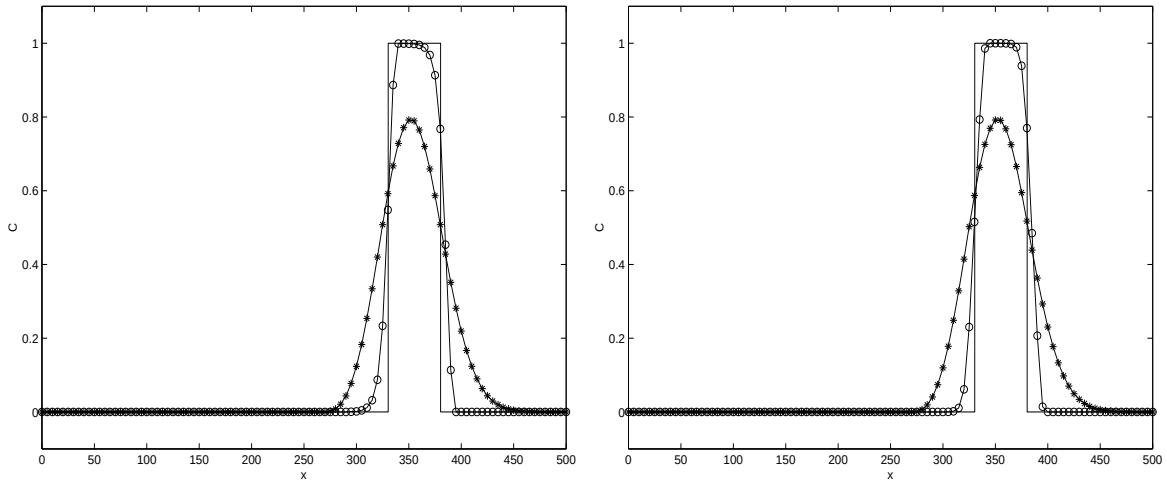

Figure 1. Concentration of pollutant for $Fr = 10$ at $t_{out} = 10s$ (left), and for $Fr = 1$ at $t_{out} = 100s$ (right). Exact solution (–), Upwind (*–), MUSCL (o–)

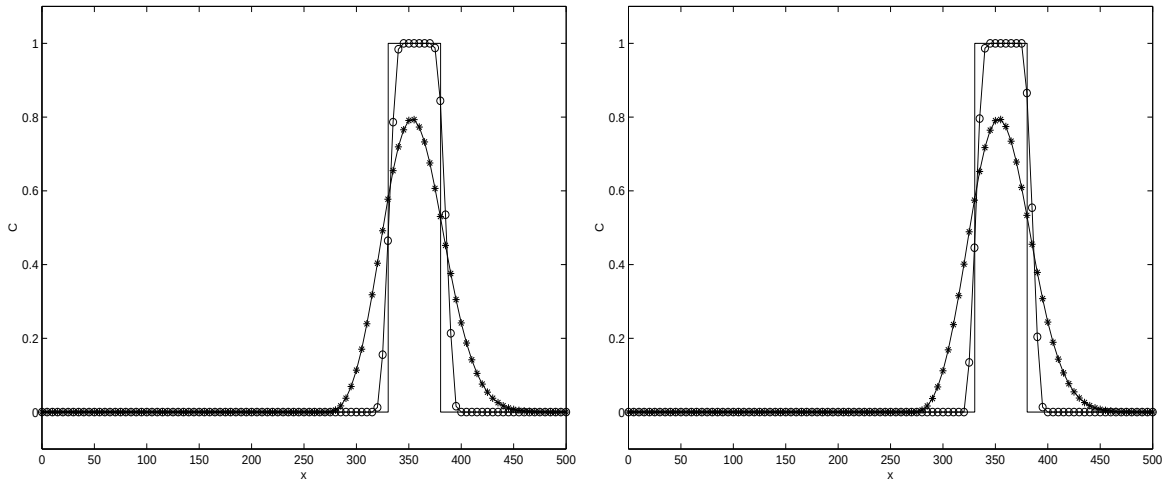

Figure 2. Concentration of pollutant for $Fr = 0.1$ at $t_{out} = 1000s$ (left), and for $Fr = 0.01$ at t_{out}=10000s (right). Exact solution (–), Upwind (*–), MUSCL (o–)

4.3. 1D dam-break problems

The first test case is of a dam break on a flat bottom, where the concentration of the pollutant has different values on each side of the dam. We compare the results with the exact solutions (presented as solid lines). For this first problem the channel length is $L = 50m$. The initial data are those of the Riemann problem, with $x_0 = 10m$ being the dam position (position of the initial discontinuity). The values of $h_L = 1m, u_L = 2.5m/s$ and $C_L = 1$ are the initial values on the left side of the dam, with right values of $h_R = 0.1m, u_R = 0m/s$ and $C_R = 0$. The simulation time is $t_{out} = 7s$. Figures 3–5 show the results for the water height, water discharge and pollutant concentration obtained using the relaxation scheme with the computational the parameters $\Delta x = 0.5m, \epsilon = 1.D - 6$, $c_1 = 6.5, c_2 = 1.4$ and $c_3 = 4$. The VL limiter was used to obtain these results. We are particularly interested in the performance of the scheme for the pollutant concentration. The numerical solution closely follows the exact one, with the pollutant shock front well captured for the coarse grid used.

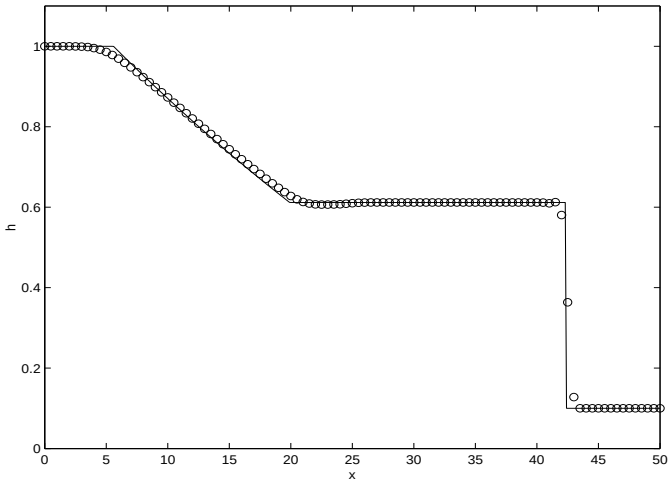

Figure 3. First dam-break problem: water height at t_{out}=7s. Exact solution (–) and MUSCL (o–)

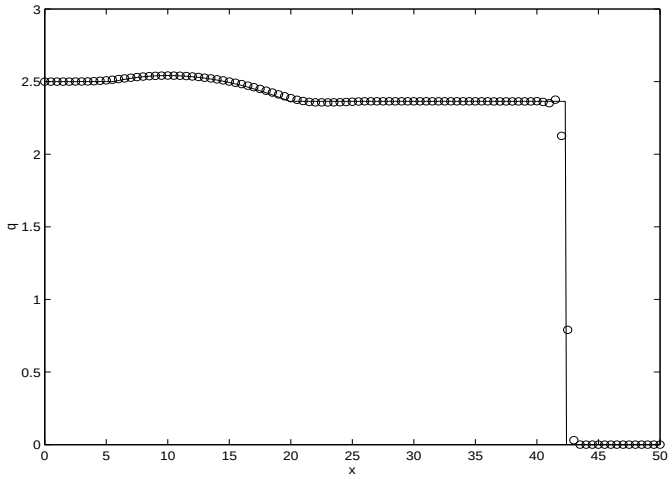

Figure 4. First dam-break problem: water discharge at t_{out}=7s. Exact solution (–) and MUSCL (o–)

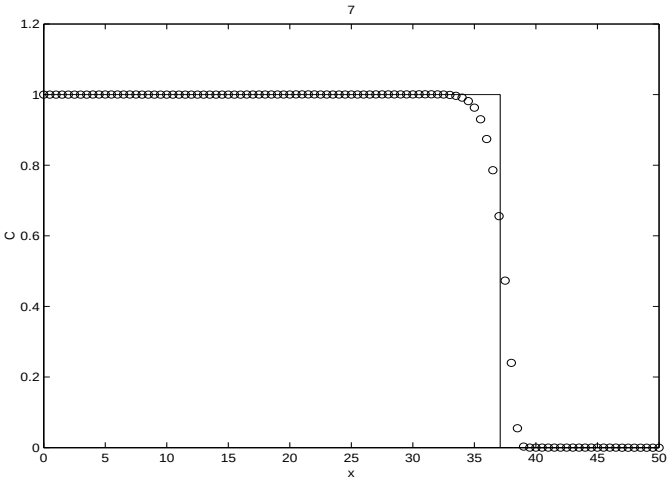

Figure 5. First dam-break problem: pollutant concentration at t_{out}=7s. Exact solution (–) and MUSCL (o–)

The second dam-break example is taken from [1] and is similar to the previous one. It is computed here in order to compare with the results presented in [1]. Here $L = 2000m$, $x_0 = 1000m$ and the initial values are $h_L = 1m, u_L = 0m/s$ and $C_L = 0.7$, $h_R = 0.5m, u_R = 0m/s$ and $C_R = 0.5$. The computational parameters used were $\Delta x = 20m, \epsilon = 1.D-6$, $c_1 = 3.5, c_2 = 3$ and $c_3 = 1$ with the VL limiter. The results are presented in Figs. 6–8 for $t_{out} = 240s$. As would be expected, the results presented in Figs. 6–8 again follow closely the exact solution and those presented in [1].

For the second dam-break problem we also present the results for the pollutant concentration for different values of h_R in Fig. 9. We chose $h_R = 0.95m$ (a very small jump) with $c_1 = 3, c_2 = 3, c_3 = 0.095$ and $h_R = 0.01m$ (a very large jump) with $c_1 = 5, c_2 = 3, c_3 = 3.5$. The speed of the pollutant shock grows as the height of the water height jump decreases. The resolution of the numerical solution for $h_R = 0.95m$ (small Fr number) is very good. For a more difficult case where $h_R = 0.01m$ the numerical solution again follows closely the exact solution.

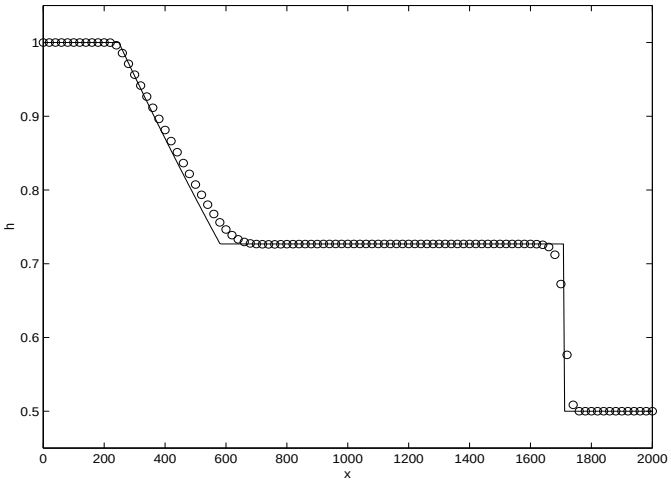

Figure 6. Second Dam Dreak problem: water height at at t_{out}=240s. Exact solution (–) and MUSCL (o–)

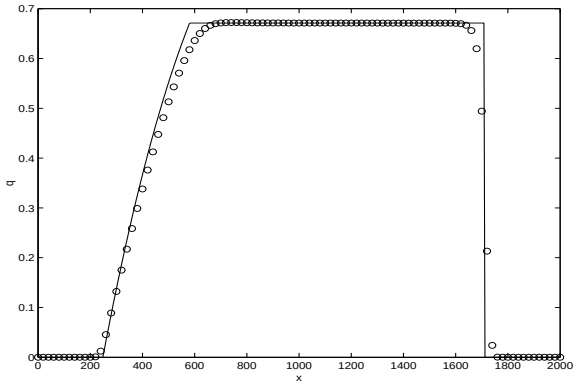

Figure 7. Second Dam Break problem: water discharge at t_{out}=240s. Exact solution (–) and MUSCL (o–)

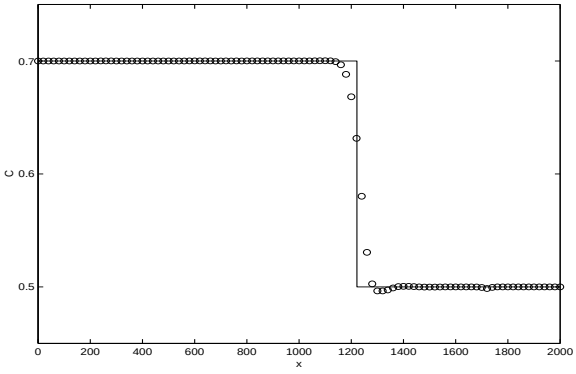

Figure 8. Second Dam Break problem: pollutant concentration at t_{out}=240s. Exact solution (–) and MUSCL (o–)

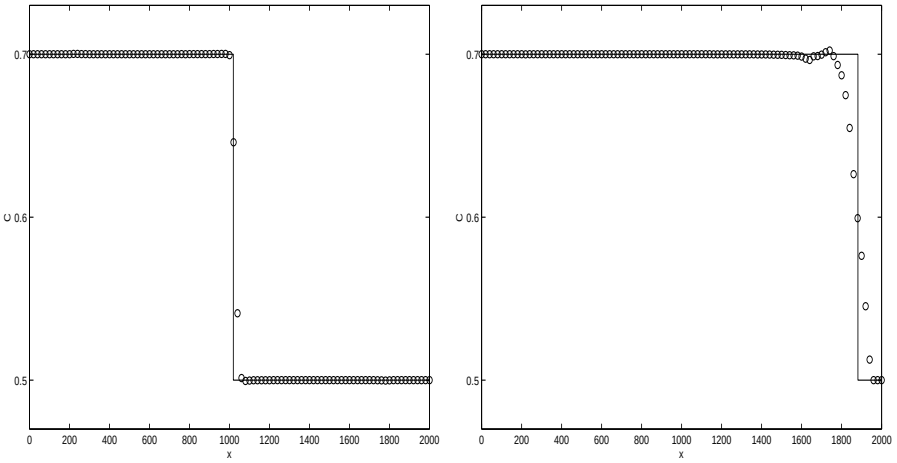

Figure 9. Second Dam Break problem: pollutant concentration for $h_R = 0.95m$ (left) and for $h_R = 0.01m$ (right), $t_{out} = 240s$. Exact solution (–) and MUSCL (o–)

4.4. Peak in the concentration of pollutant

This test problem was also presented in [1], as to test the scheme when the concentration of pollutant has rapid oscillations. The initial data is still a dam-break problem with the same values as in the first example in the previous section, with the exception of a peak in the initial pollutant concentration just before the jump. So $C_I(x,0) = 0.9$ for $x \in I = [900, 1000]$. There in no exact solution for this problem. On the other hand we know that the initial value at $x_0 = 1000$ will be simply transported to the right with its maximum value staying equal to C_I. In Figure (10) the numerical result is presented at $t_{out} = 250s$ along with the initial data. Using $\Delta x = 20m, \epsilon = 1.D-8$, $c_1 = 4 = c_2$ and $c_3 = 2.5$ with the VL limiter, the scheme computes exactly the exact maximum concentration with small diffusion added in the overall solution, comparing well with the result presented in [1].

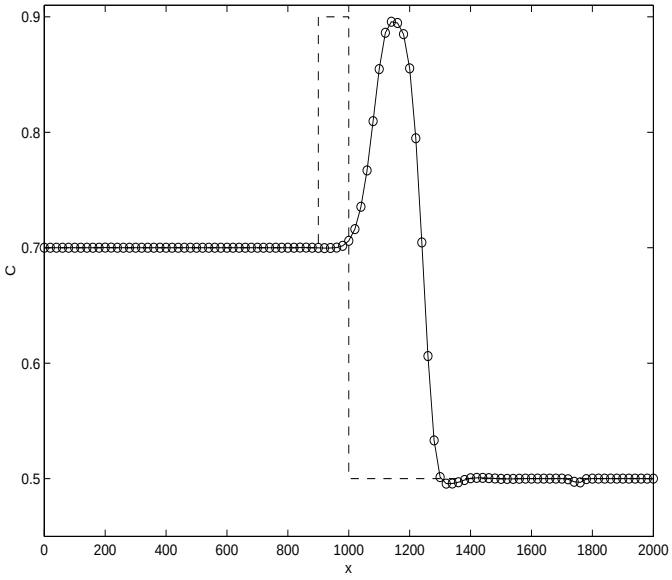

Figure 10. Concentration of the pollutant for the peak problem. Initial concentration (- -) and concentration at $t_{out} = 250s$ for the MUSCL relaxation scheme (o–).

4.5. A two rarefaction problem

This test problem is due to [17] and has initial data as to produce two strong rarefaction waves travelling in opposite directions. Here $L = 50m$, $x_0 = 25m$, the initial values are $h_L = 1m, u_L = -5m/s$ and $C_L = 1$, $h_R = 1m, u_R = 5m/s$ and $C_R = 0$. At $t_{out} = 2.5s$ the water depth in the middle of the two rarefaction waves becomes very shallow (nearly dry). It is well known that a large class of schemes will compute a negative depth in the vicinity of a very shallow water depth and this may lead to problems when one wants to calculate the pollutant concentration. For this test, the exact solution for the pollutant concentration is that of the stationary contact discontinuity, which is very difficult to calculate exactly as a perfect discontinuity by most schemes (see [17]). The results for the relaxation scheme are presented in Figs. 11–13, using $\Delta x = 0.5m, \epsilon = 1.D-6$, $c_1 = 6 = c_2$ and $c_3 = \min_i u_i$ with the VL limiter. While the resolution of the solutions for h and q is in very good agreement with the exact solution, the stationary contact discontinuity is poorly resolved. Nevertheless, the result obtained is better than those obtained by other schemes and has almost the correct

behavior. This is a limitation of the relaxation scheme presented, since it has no inherent property to deal with this situation. This is an interesting problem which can benefit from further investigations, possibly in the line of the works in [1, 5].

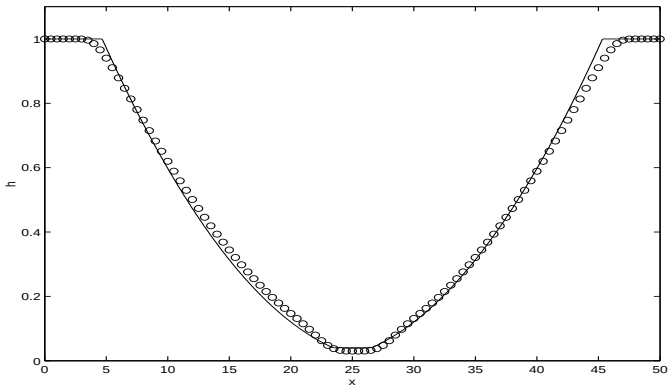

Figure 11. Two rarefaction problem: water height at $t_{out} = 2.5s$. Exact solution (–) and MUSCL (o–)

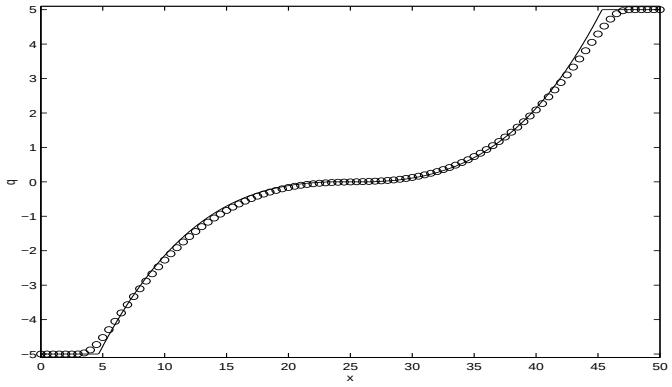

Figure 12. Two rarefaction problem: water discharge at $t_{out} = 2.5s$. Exact solution (–) and MUSCL (o–)

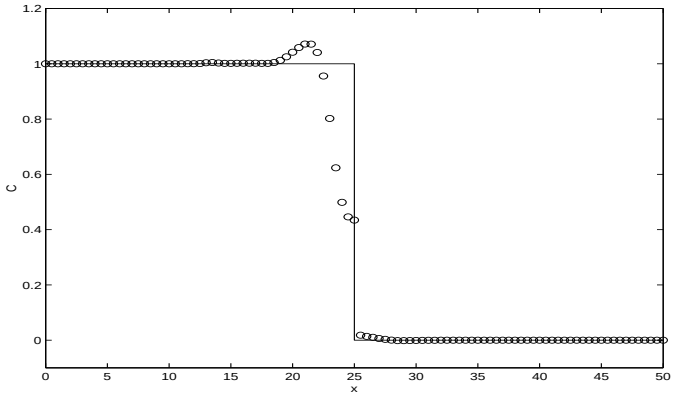

Figure 13. Two rarefaction problem: pollutant concentration at $t_{out} = 2.5s$. Exact solution (–) and MUSCL (o–)

4.6. Advection of pollutant over topography

In this example, we assume that the initial water level is constant, i.e., $h + Z = 1$, the initial discharge $q = 0.1$ and the gravitational constant is $g = 1$, with $L = 1m$ and the bottom

topography $Z(x)$ given by the hump

$$Z(x) = \begin{cases} 0.25(\cos(10\pi(x-0.5))+1), & 0.4 \leqslant x \leqslant 0.6, \\ 0, \quad \text{otherwise.} \end{cases}$$

The initial polluted area is $I = [0.4, 0.5]$ with $C_I(x,0) = 1$, with no pollution source turned on.

As the solution evolves in time, the initial pollutant concentration propagates downstream. We compute the concentration starting at $t = 0s$ at times $t_{out} = 2s, 4s$. Using $\Delta x = 0.005m, \epsilon = 1.D-6$, $c_1 = 1 = c_2$ and $c_3 = 0.2$ with the MC limiter, we can observe in Fig. 14 that at $t_{out} = 2$ the initial concentration has just passed through the bottom hump while retaining its maximum value, with no visible distortions of the solution, which is only slightly diffused. At time $t_{out} = 4$ the concentration layer has propagated further to the right while still retaining its maximum value. We can conclude that the interaction with the nonflat bottom has not resulted in any nonphysical behavior for the solution, such as numerical oscillations or negative values. Similar observations will be made in the next test case.

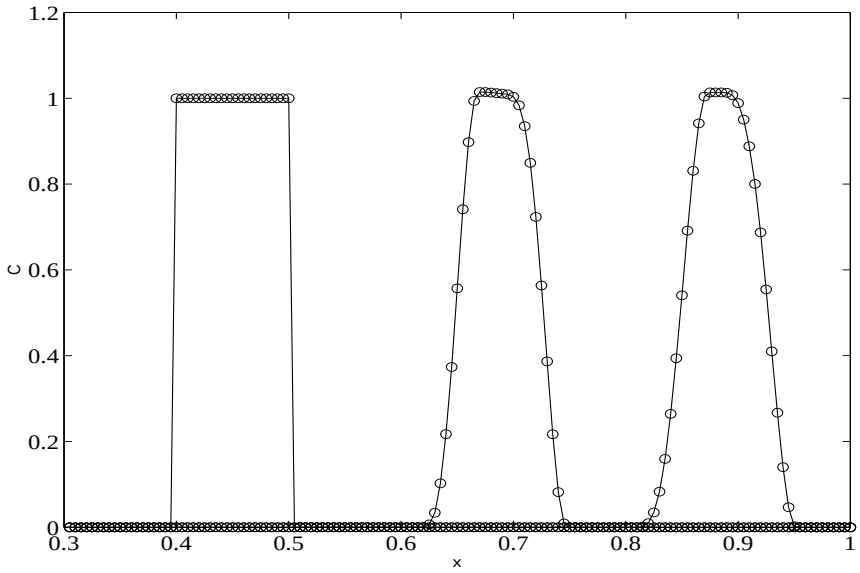

Figure 14. Advection of Pollutant Over Topography: concentration of the pollutant, at times $t_{out} = 0s, 2s, 4s$ from left to right for the MUSCL relaxation scheme

4.7. Emission of pollutant over topography

This test case is also from [1]. Here we test the introduction of a source of pollutant into a flow. For this problem, the initial data are $h + Z = 2$, $q = 0.5$ with $L = 1000m$ and $g = 1$ with

$$Z(x) = \begin{cases} 0.2 - 0.05(x-10)^2, & 8 \leqslant x \leqslant 12, \\ 0, \quad \text{otherwise.} \end{cases}$$

We assume that the water is initially clean until the time $t_b = 100s$ (the flow has reached a steady state at this point) when a source of water $\Sigma = 0.01$ with a concentration of pollutant

$C_\Sigma = 10$ is turned on at the point $x = 45m$, then at the time $t_e = 300s$ the pollution source is turned off. Then we follow the evolution of this pollutant layer.

For $\Delta x = 4m, \epsilon = 1.D-6$, $c_1 = 2, c_2 = 1$ and $c_3 = 0.5$ with the MC limiter, the numerical results for the pollutant concentration are presented in Figs. 15 and 16 at times $t_{out} = 300s, 350s, 500s$ and $800s$, for the interval $I = [0, 500]$. The results are in very good agreement with those presented in [1, 4]. As pointed out in [1], due to the presence of the water source there is a local modification in space and time of the hydrodynamic computation. Here we prove that the relaxation scheme can cope with such situations, producing reliable results.

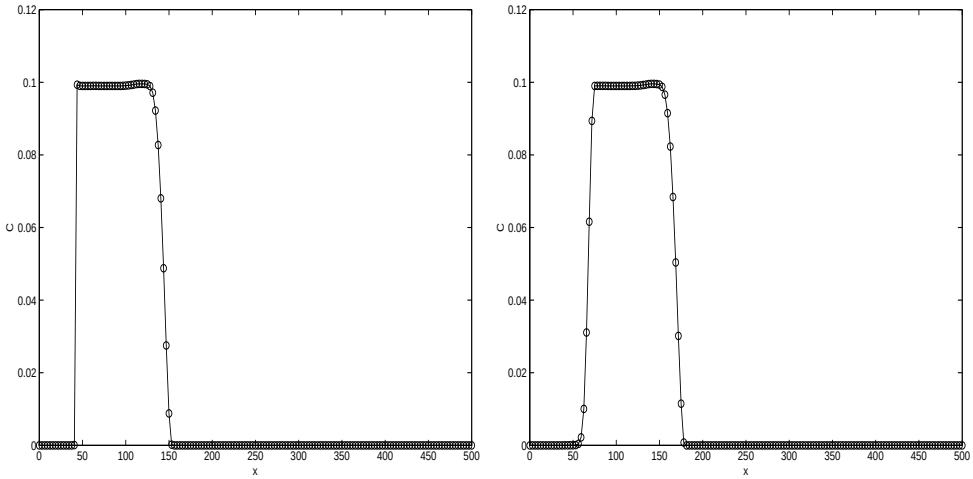

Figure 15. Emission of Pollutant Over Topography: concentration of the pollutant at times $t = 300s$ (left) and $t = 350s$ (right) for the MUSCL relaxation scheme

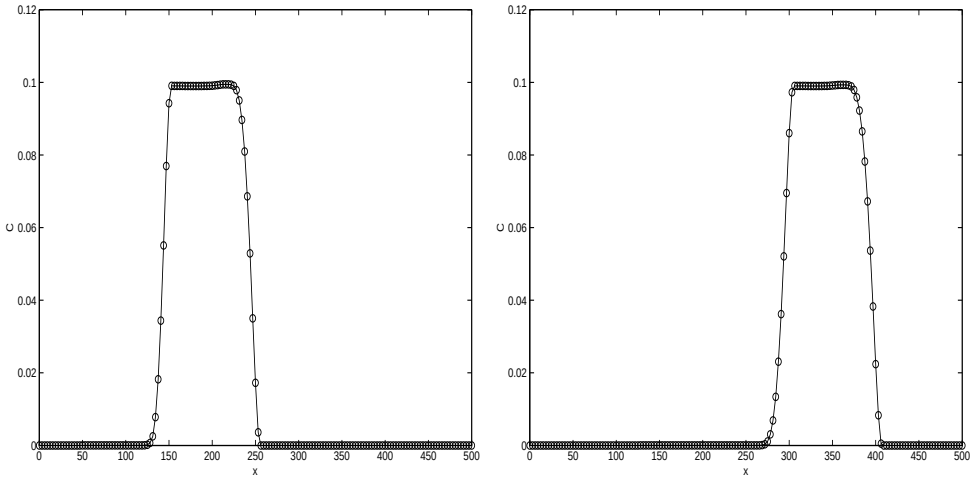

Figure 16. Emission of Pollutant Over Topography: concentration of the pollutant at times $t = 500s$ (left) and $t = 800s$ (right) for the MUSCL relaxation scheme

5. 2D numerical tests and results

In this section, we apply the relaxation scheme to two-dimensional problems. We will not make a complete presentation of the extension of the scheme in 2D here, since it will be

detailed elsewhere. The 2D computations are based on extending the 1D strategy.

We will just present the 2D relaxation model that corresponds to equation (5) for the 1D case. Considering the classical 2-D conservation law

$$\begin{gathered}\frac{\partial \mathbf{u}}{\partial t}+\frac{\partial \mathbf{f}(\mathbf{u})}{\partial x}+\frac{\partial \mathbf{g}(\mathbf{u})}{\partial y}=\mathbf{s}(\mathbf{u}); \quad (x,y)\in\mathbb{R}^2,\ t>0,\\ \mathbf{u}(x,y,0)=\mathbf{u}_0(x,y); \quad (x,y)\in\mathbb{R}^2\end{gathered} \tag{21}$$

with $\mathbf{u},\mathbf{f}(\mathbf{u})$ and $\mathbf{g}(\mathbf{u})\in\mathbb{R}^n$, we introduce the relaxation variables $\mathbf{v},\mathbf{w}$ to (21), and the linear relaxation model in 2D reads as follows:

$$\begin{aligned}\frac{\partial \mathbf{u}}{\partial t}+\frac{\partial \mathbf{v}}{\partial x}+\frac{\partial \mathbf{w}}{\partial y}&=\mathbf{s}(\mathbf{u}),\\ \frac{\partial \mathbf{v}}{\partial t}+\mathbf{C}^2\frac{\partial \mathbf{u}}{\partial x}&=-\frac{1}{\epsilon}(\mathbf{v}-\mathbf{F}(\mathbf{u}))\\ \frac{\partial \mathbf{w}}{\partial t}+\mathbf{D}^2\frac{\partial \mathbf{u}}{\partial y}&=-\frac{1}{\epsilon}(\mathbf{w}-\mathbf{G}(\mathbf{u})),\end{aligned} \tag{22}$$

where now $\mathbf{C}^2,\mathbf{D}^2\in\mathbb{R}^{n\times n}$ are positive diagonal matrices. In the limit $\epsilon\to 0^+$ system (22) approaches the original system (1) by the *local equilibrium* $\mathbf{v}=\mathbf{F}(\mathbf{u})$ and $\mathbf{w}=\mathbf{G}(\mathbf{u})$. A general necessary condition for such convergence is that a subcharacteristic-like condition is satisfied. For system (22) we require that

$$\frac{\lambda_i^2}{c_i^2}+\frac{\mu_i^2}{d_i^2}\leqslant 1, \quad \forall i \tag{23}$$

with λ_i,μ_i being the eigenvalues of $\partial\mathbf{F}(\mathbf{u})/\partial\mathbf{u}$ and $\partial\mathbf{G}(\mathbf{u})/\partial\mathbf{u}$ respectively.

5.1. 2D dam-break peak problem

This problem is similar to the 1D problem presented in Section 4.4, and similar to the one presented in [1]. The initial data are the same as for the problem in Section 4.4, except that $L=1m$, $t_{out}=0.1s$. The channel width is $0.1m$. The solution is very close to the 1D solution and the data are invariant in the y-coordinate.

We compare the first-order upwind relaxation and the second-order MUSCL relaxation schemes. We use a uniform mesh with $\Delta x=\Delta y=0.01$ and computational parameters $\epsilon=1.D-6$, $c_1=4=c_3, c_2=1=c_4$ and $d_1=4=d_3, d_2=0.01=d_4$ for both schemes. The initial data for the pollutant concentration and the computed results are presented in Figs. (17)–(19). With the upwind schemes the results are diffusive, while the MUSCL scheme uniformly preserves the peak value of the pollutant concentration.

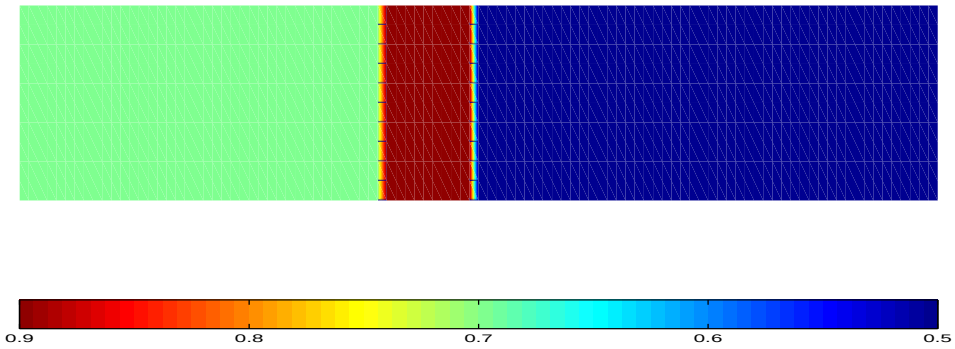

Figure 17. Initial data for the pollutant concentration of the 2D dam-break problem

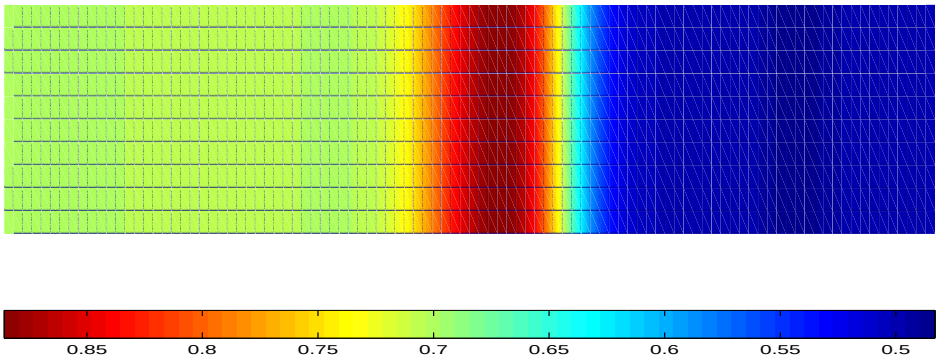

Figure 18. Pollutant concentration computed with the upwind scheme for the 2D dam-break problem and at $t_{out} = 0.1s$

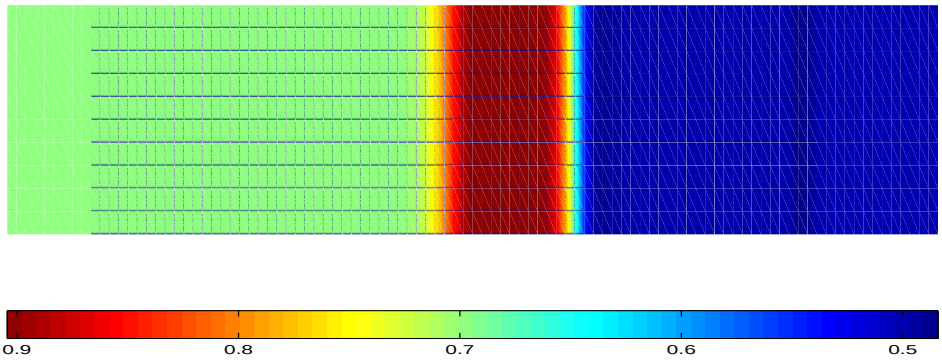

Figure 19. Pollutant concentration computed by the MUSCL relaxation scheme for the 2D dam-break problem and at $t_{out} = 0.1s$

5.2. 2D partial dam-break

This problem is similar to the one considered in [5] and is the case of a 2D square domain $1400m \times 1400m$, where the water flows from the left to the right through a breach located

between $y = 560$ and $y = 840$. The initial data are $u_L = u_R = v_L = v_R = 0$ and $h_L = 0.5m$ and $h_R = 1m$. The initial pollutant concentration is given by

$$C(x, y, 0) = \begin{cases} e^{-0.0001[(x-650)^2+(y-600)^2]}, & 0 \leqslant x \leqslant 700, 0 \leqslant y \leqslant 1400 \\ 0.5 & 700 \leqslant x \leqslant 1400, 0 \leqslant y \leqslant 1400. \end{cases}$$

The boundary conditions at $x = 0$ and $x = 1400m$ are assumed to be transmissive and all the other boundaries are considered as reflective. At the instant of breaking of the dam, water is released through the breach, forming a positive wave propagating downstream and a negative wave spreading upstream. The computational parameters used were $\epsilon = 10^{-6}$ and $c_1 = 10, c_2 = 6, c_3 = 11, d_1 = 10, d_2 = 5, d_3 = 11$. The VL limiter was applied in all computations. The solution computed on a 500×500 grid at time $t_{out} = 200s$ is shown in Figs. 20 and 21. The scheme provides a very high resolution of the circular shock wave and the vortices formed on the breach. The results for the pollutant concentration correctly describe the physical behavior and are comparable to those presented in [5].

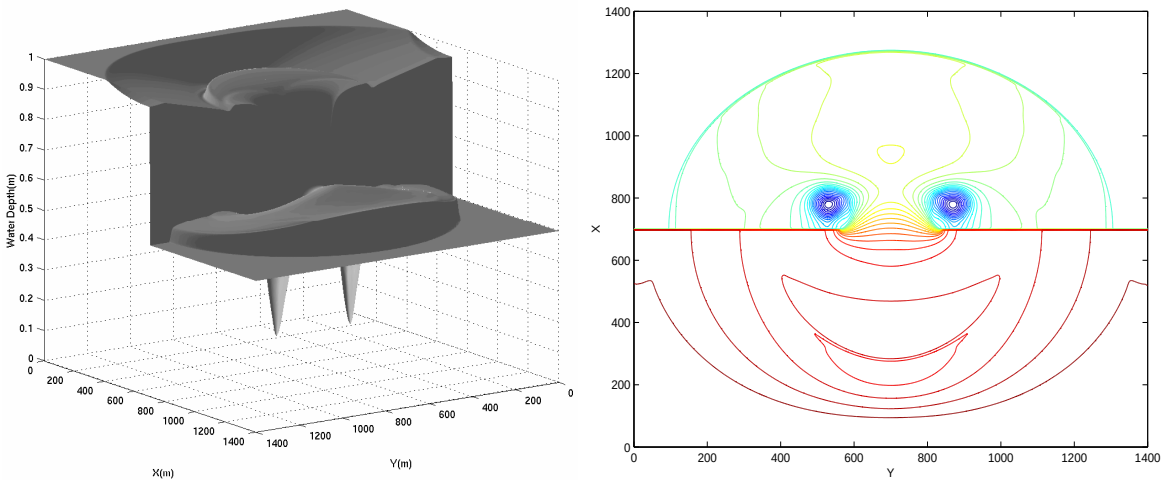

Figure 20. 2D partial dam-break: 3D plot (left) and contour plot (right) for the water height at $t_{out} = 200s$ computed by the MUSCL relaxation scheme

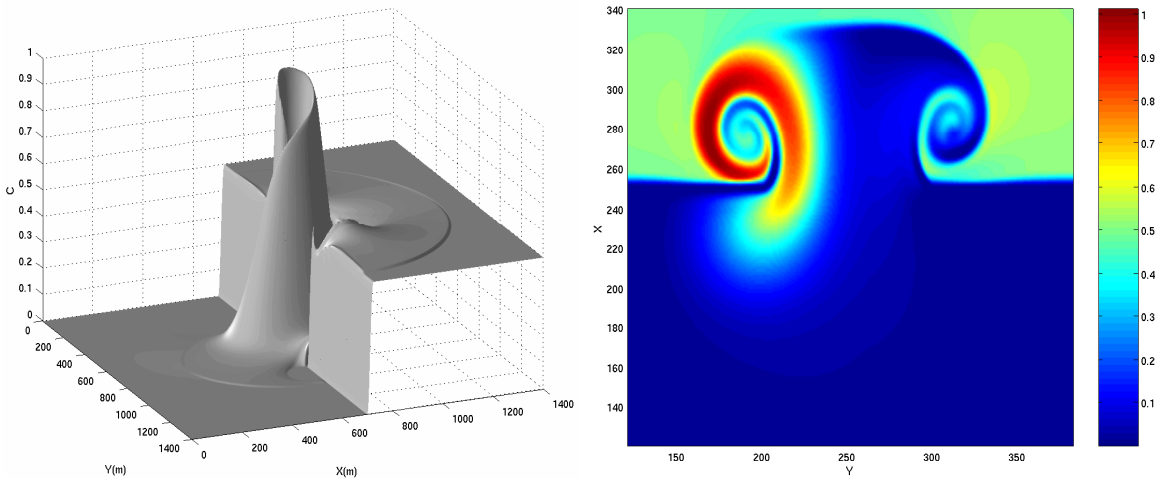

Figure 21. Partial dam-break: 3D plot (left) and magnified top view (right) for the pollutant concentration $t_{out} = 200s$ computed by the MUSCL relaxation scheme

5.3. Emission of pollutant in a reservoir

This test problem is to simulate the transport and diffusion in a reservoir. The computational domain is a $200m \times 200m$ region subdivided into an 81×81 square grid. The initial stagnant water depth in the reservoir is $h = h_L = 1m = h_R$ and $u_1 = u_2 = 0$, with no pollutant present inside the domain. The values of the diffusion coefficients are $D_x = D_y = 29.2m^2/s$. A breach exists, it is located in the middle of the reservoir, and is $75m$ in length, having distances of 30m from the left bank and 95m from the right. The boundary conditions at $x = 0$ and $x = 200m$ are assumed to be transmissive and all the other boundaries are considered as reflective. At the beginning at the inlet of the reservoir we impose $u_1 = 0.1m/s$ and a pollutant is released with $C = 0.7$. The computational parameters used were $\epsilon = 1.D-6$ and $c_1 = c_3 = 4, c_2 = c_4 = 0.25, d_1 = d_3 = 4, d_2 = d_4 = 0.15$, with the MC limiter. The results for two consecutive representations in terms of velocity fields and pollutant concentration distribution are presented in Figs. 22 and 23. We can clearly see the discharge effect on the evolution of the pollutant concentration on the initially stagnant reservoir water.

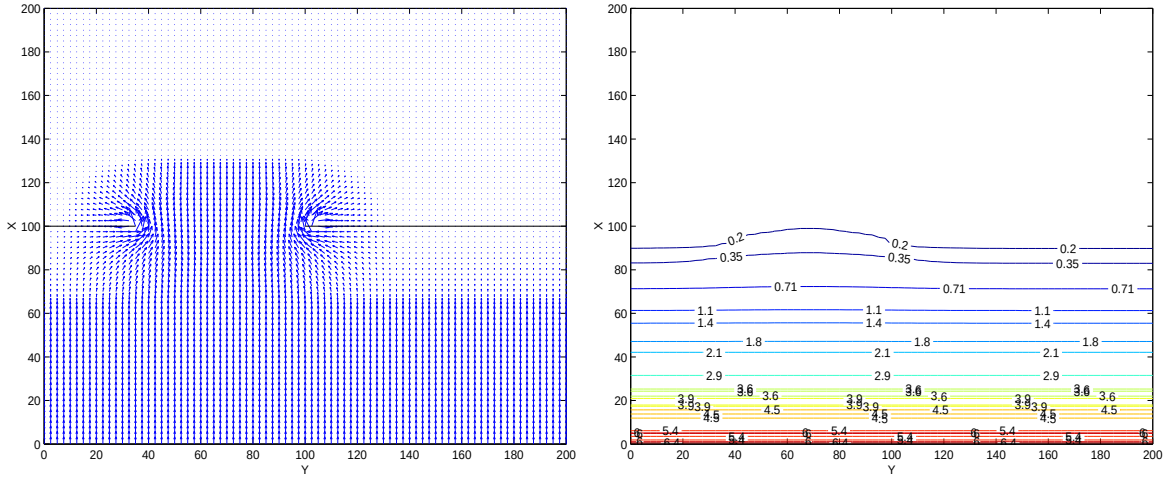

Figure 22. Emission of pollutant in a reservoir: velocity field (left) and pollutant concentration contours (right) at time $t = 40s$ computed by the MUSCL relaxation scheme

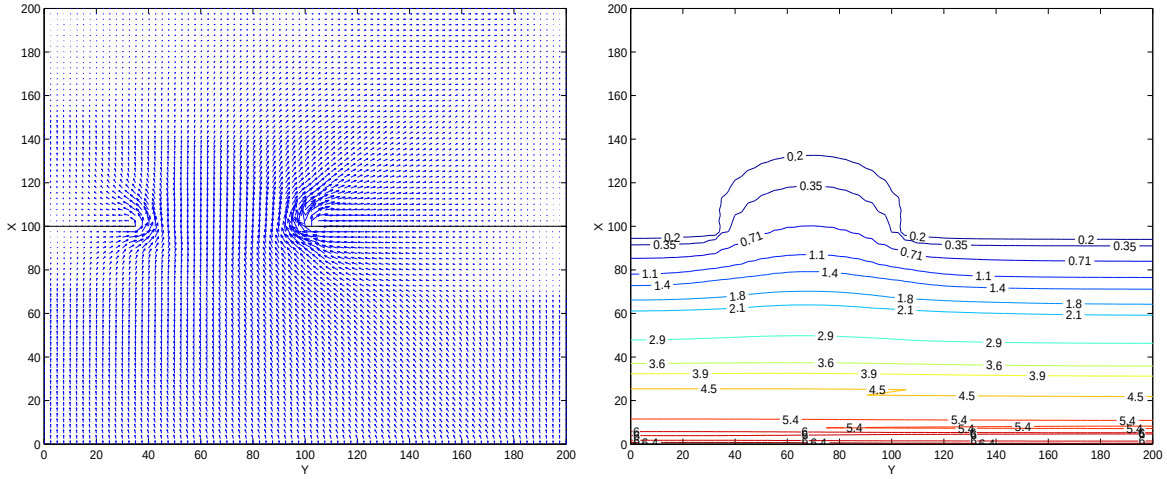

Figure 23. Emission of pollutant in a reservoir: velocity field (left) and pollutant concentration contours (right) at time $t = 80s$ computed by the MUSCL relaxation scheme

6. Conclusions

In the present work, relaxation schemes have been rigorously studied in order to compute the transport and diffusion of a pollutant in shallow water flows with and without source terms present. The main feature of the schemes is their simplicity and robustness. Finite volume shock capturing spatial discretizations, that are Riemann solver free, have been used to provide an accurate shock resolution and pollutant advection and diffusion. Some of the limitations of the schemes are also presented, they require further research. The schemes have been extended in two dimensions. The benchmark tests have shown that the schemes provide accurate solutions that are in good agreement with analytical or reference solutions. The results also demonstrate that the relaxation schemes are accurate, simple, efficient and robust and can be of practical consideration and need further study and development.

References

[1] E. Audusse and M. O. Bristeau, *Transport of pollutant in shallow water. A two time steps kinetic method*, M2AN Math. Model. Numer. Anal., **37** (2003), pp. 389–416.

[2] P. Brufau and P. Garcia-Navarro, *Unsteady free surface flow simulation over complex topography with a multidimensional upwind technique*, J. Comp. Phys., **186** (2003), pp. 503–526.

[3] A. Chalabi, *Convergence of relaxation schemes for hyperbolic conservation laws with stiff source terms*, Math. Comput., **68** (1999), pp. 955–970.

[4] A. Chertock, A. Kurganov and G. Petrova, *Finite Volume Particle Methods for Models of Transport of Pollutant is Shallow Water*, (to appear in) J. Sci. Comput, (2005)

[5] A. Chertock and A. Kurganov, *On a Hybrid Finite-Volume-Particle Method*, (to appear in) M2AN Math. Model. Numer. Anal., (2005)

[6] A. I. Delis, *Improved application of the HLLE Riemann solver for the shallow water equations with source terms*, Comm. Numer. Meth. Eng., **39** (2003), pp. 59–83.

[7] A. I. Delis and Th. Katsaounis, *Relaxation schemes for the shallow water equations* Int. J. Numer. Meth. Fluids, **41** (2003), pp. 695–719.

[8] T. Gallouët, J. M. Herard and N. Seguin, *Some approximate Godunov schemes to compute shallow water equations with topography*, Computers and Fluids, **32** (2003), pp.479–513.

[9] P. Garcia-Navarro and M. E. Vázquez-Cendón, *On numerical treatment of the source terms in the shallow water equations*, Computers and Fluids, **29** (2000), pp. 951–979.

[10] S. Jin, *A steady-state capturing method for hyperbolic systems with geometrical source terms*, M2AN Math. Model. Numer. Anal., **35** (2001), pp. 631–646.

[11] S. Jin and Z. Xin, *The relaxing schemes of conservations laws in arbitrary space dimensions* Comm. Pure Appl. Math., **48** (1995), pp. 235–277.

[12] Th. Katsaounis and C. Makridakis, *Relaxation models and finite element schemes for the shallow water equations* Hyperbolic problems: theory, numerics, applications, Springer, Berlin (2003), pp. 621–631.

[13] A. Kurganov and L. Levy L, *Central-upwind schemes for the Saint-Venant system*, M2AN Math. Model. Numer. Anal., **36** (2002), pp. 397–451.

[14] R. J. LeVêque, *Finite Volume Methods for Hyperbolic Problems*, Cambridge University Press, 2002.

[15] R. Natalini, *Convergence to equilibrium for the relaxation approximations of conservation laws*, Comm. Pure Appl. Math., **49** (1996), pp. 795–823.

[16] B. Perthame and C. Simeoni, *A kinetic scheme for the Saint–Venant system with a source term* CALCOLO, **37** (2001), pp. 201–231.

[17] E. F. Toro, *Shock-capturing methods for free-surface shallow flows*, Wiley, 2001.

Received 2 Sep. 2004